

OMAE2015-41350

EVALUATION OF THE CSR-H SLOSHING CRITERION USING DIRECT FLUID STRUCTURE CALCULATION

Po-Wen Wang*

Chi-Fang Lee

Yann Quéméner

Chien-Hua Huang

Research Department
CR Classification Society
Kobe, Japan

ABSTRACT

The objective of this study was to clarify the theoretical basis of sloshing loads and required plate thickness formulations in the harmonized common structural rules. This study used computational fluid dynamic (CFD) to calculate sloshing loads and used finite element analyses (FEA) to evaluate structural response. The sensitivity of the CFD predictions to the time step and grid size was also investigated. Cargo oil tanks were then selected in a handy size oil tanker and a very large crude carrier to evaluate the longitudinal and transverse sloshing loads on the tank boundaries. The results showed that the sloshing pressures computed at four filling levels were mostly consistent with CSR-H. Afterward, the sloshing pressure produced by CFD was applied to the finite element model by using a fluid-structure interaction technique to obtain the dynamic response of the structure. The dynamic responses were investigated to validate the quasistatic approach for sloshing assessment.

Keywords: sloshing, computational fluid dynamics (CFD), finite element analyses (FEA), Harmonised Common Structural Rules (CSR-H)

1. INTRODUCTION

The configuration of partially filled tanks enables the movements of liquid cargo generated by the ship motion and induces loads on the tank boundaries. Although oil tankers mostly operate with either full or empty tanks, the partially filled condition must be considered to verify that the integrity of the tank structure is ensured for any possible load configurations. The sloshing phenomenon occurs when the external excitation frequency is close to the natural frequency of the liquid motion inside the tank. The sloshing can thus generate transiently high peaks of pressure on the tank boundaries, and such pressure can cause local structural damage. Sloshing has recently become more critical because the size of very large crude carriers (VLCCs) and liquefied

natural gas (LNG) carriers tends to increase, thus leading to larger cargo tanks with a lower natural frequency. Large tanks are thus more likely to be subjected to sloshing because the natural frequency of the tank corresponds to ship motions in more probable sea state.

Sloshing is a complex phenomenon involving fluid motion with high nonlinearity and randomness. In recent years, the development of computational fluid dynamic (CFD) methods has matured and been widely applied in the industry, particularly regarding ship systems. Several researchers have addressed the sloshing problem by validating numerical predictions with experimental data. Sames et al [1] successfully simulated sloshing in rectangular and cylindrical tanks by using the Comet CFD software and a simplified 2D modeling approach. Moirod et al [2] simulated sloshing in LNG tanks by using CFD software (Flow3D and OpenFOAM) and a 3D modeling approach with idealized smooth tank boundaries. The simulation results were consistent with the experimental outcomes. Finally, Jeon et al [3] examined the effect of cross-ties in a VLCC cargo tank by using the CFD software STAR-CCM+ and a complex 3D model of the tank that included the geometry of the transverse members. Their predictions were consistent with the experimental outcomes. Therefore, this study used the CFD approach to evaluate the sloshing load in tanks.

Because of the transient character of the pressures on the tank boundaries generated by the sloshing, the structure can respond dynamically, leading to a dramatic level of stress locally. Fossa et al [4] and Ganuga et al [5] performed a fluid structure interaction (FSI) analysis to examine the dynamic structural response to sloshing loads. In addition, Pozarlik et al [6] compared the one-way and two-way FSI methods and concluded that the one-way interaction enabled accurate prediction of the dynamic structural response in a reasonable computation time. However, CSR-H [7] considered a

quasistatic response of the structure subjected to sloshing loads. This study thus examined the structural response of several cargo oil tanks by conducting one-way FSI analysis.

This paper comprises three sections. The first section presents the sloshing load assessment by direct hydrodynamic analysis and by the rules. The second section presents evaluations of the sloshing pressure in three cargo oil tanks. The third section examines the structural response to sloshing by conducting FSI analysis.

2. SLOSHING LOADS ASSESSMENT

2.1 Direct assessment approach through CFD

This study used the STAR-CCM+ CFD software to perform a CFD analysis to simulate the sloshing in tanks. STAR-CCM+ enables to generate a mesh of the volume enclosed in the tank and to simulate the flow during the analysis. This study adopted the finite volume method to discretize the governing equations by subdividing the fluid domain into an arbitrary number of contiguous cells. The values of all dependent variables stored refer to the center of each cell. The volume and surface integrals were calculated using a second-order upwind scheme with second-order precision. This study used the standard k- ϵ turbulence model to examine the viscous flow.

To simulate the free surface behavior, this study used the volume-of-fluid (VoF) method, which involves mixing two fluids, using the volume fraction parameter c expressed in Eq. (1).

$$c = \frac{V_w}{V} \quad (1)$$

where V is the total volume of the cell and V_w is the volume of liquid in the cell.

Equations (2) and (3) can be used to compute the combined density and viscosity that are necessary required to solve the multiphase flow problem expressed in Eq. (4).

$$\rho = c \cdot \rho_w + (1 - c) \rho_a \quad (2)$$

$$\mu = c \cdot \mu_w + (1 - c) \mu_a \quad (3)$$

$$\frac{\partial c}{\partial t} + \vec{v} \cdot \nabla c = 0 \quad (4)$$

where ρ is the density, μ is the dynamic viscosity coefficient, and the indices w and a stand for water and air, respectively.

Figure 1 shows the two-phase fluid domain (i.e. water and air) modeled through cells. The free surface was initially located so that $c_a=c_w=0.5$.

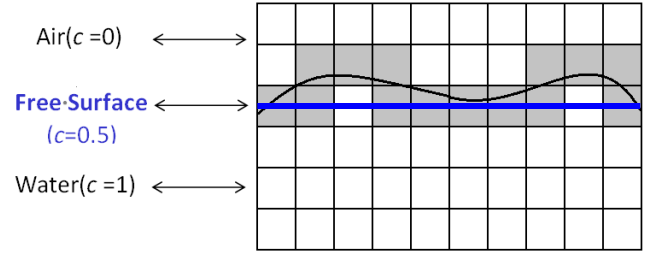


Figure 1. FREE SURFACE VOF REPRESENTATION.

2.2 CFD modeling calibration

To validate the computational model, this study calibrated the CFD settings by reproducing the sloshing loads in a rectangular tank for which the experimental results were reported by the SPH European Research Interest Community [8]. Figure 2 shows the examined rectangular tank that had a filling ratio h/H of 18%. The tank was subjected to a periodic rolling motion around the z axis centered at the origin (Fig. 2), as expressed in Eq. (5).

$$\theta = \theta_0 \sin \omega t \quad (5)$$

where θ is the angular position at time t , θ_0 is the maximum roll angle corresponding to 0.069rad (i.e., approximately 4°) and ω is the rolling frequency assumed as 3.856 rad/s.

As illustrated in Fig. 2, the sensor was positioned identically to the experiment [8] to record the liquid pressures during the simulation. For the CFD analysis, the grid size of the fluid domain must be small enough to reproduce precisely the free surface behavior during the sloshing without affecting the computation time dramatically. Therefore, this study initially set the mesh size at 0.005 m, which corresponds to 100 elements through the depth of the tank.

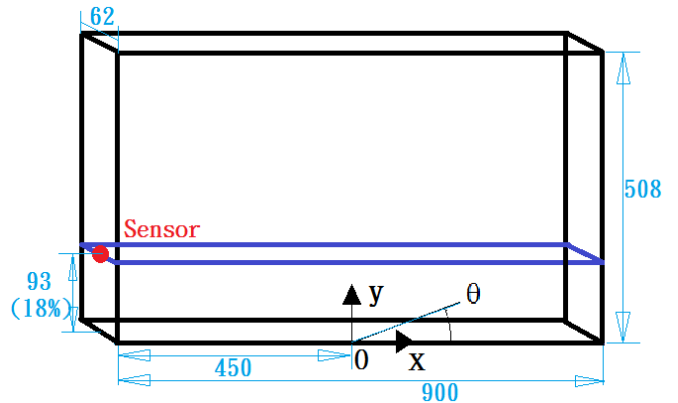


Figure 2. GEOMETRY OF THE RECTANGULAR TANK.

First, this study investigated the effect of the time step on the numerical results. The simulations were thus conducted for three different time steps $\Delta t = \{0.005s, 0.001s, 0.0005s\}$. Figure 3 shows the evaluated pressure over the simulation time. The solid line represents the evolution of the pressure measured

during the experiment [8]. The dashed lines indicate the numerical results obtained for the three different time steps. As shown in this figure, the numerical and experimental results demonstrate similarly shaped double pressure peaks where the first peak was higher and lasted a shorter time than the second peak did. This is representative of the flapping phenomenon during which the fluid crest first hits the wall before the remaining fluid reaches it. The CFD can thus precisely reproduce this highly nonlinear pressure impact of the crest and subsequent fluid dynamic pressure. The three time step settings were adequate to reproduce accurately the second pressure peak generated by the fluid dynamic pressure. However, the first peak value was more accurately reproduced by the time step $\Delta t = 0.001$ s. Therefore, this study adopted this time step for the CFD analysis.

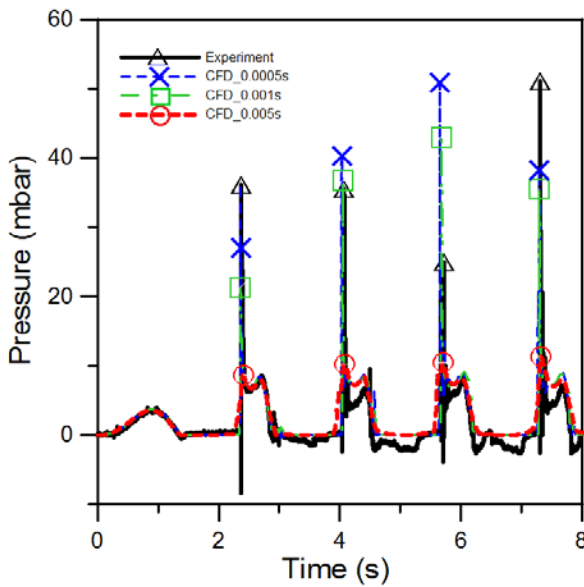


Figure 3. CFD SLOSHING PRESSURE PREDICTION FOR VARIOUS TIME STEP SETTINGS.

Figure 4 shows the tank free surface behavior during four sloshing instances simulated using a time step Δt of 0.001 s. Traveling waves at $t = 1.92$ s and hydraulic jump at $t = 2.95$ s were observed under a low filling condition. The breaking waves caused by the impact on the wall at $t = 3.97$ s was also observed. Figures 5 and 6 show a comparison of the numerical and experimental results regarding the free surface contour when the phenomenon of overturning surface occurred ($t = 3.75$ s) and when the wave broke over the wall ($t = 5.75$ s), respectively. The similarity between the CFD predictions and experimental observations validated the time step setting.

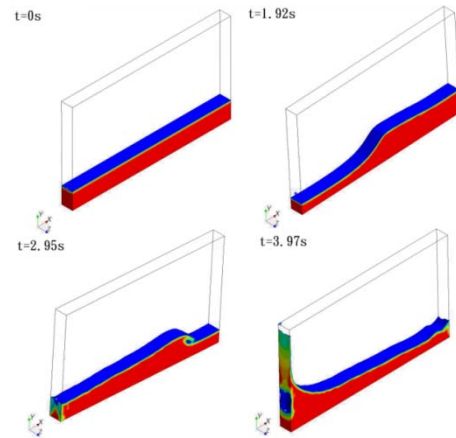


Figure 4. LIQUID FREE SURFACE DURING SLOSHING.

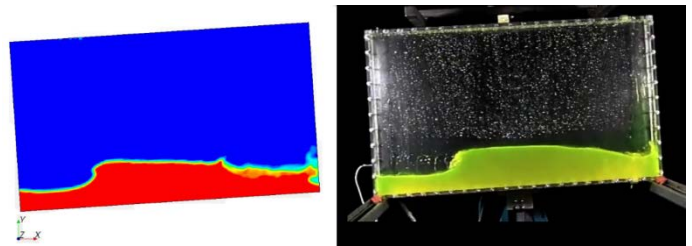


Figure 5. LIQUID FREE SURFACE CONTOUR AT $t=3.75$ s.

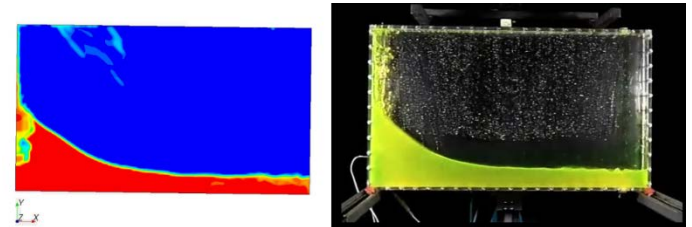


Figure 6. LIQUID FREE SURFACE CONTOUR AT $t=5.75$ s.

This study subsequently investigated the effect of grid size on the numerical results. Simulations were thus conducted for three different grid sizes:

- A coarse grid size of 0.01 m corresponding to 50 elements over the depth of the tank,
- A medium grid size of 0.008 m corresponding to 70 elements over the depth of the tank, and
- A fine grid size of 0.005 m corresponding to 100 elements over the depth of the tank.

The time step was set at 0.001 s, as previously established. Figure 7 illustrates the pressure evaluated through the simulation. The solid line represents the evolution of the pressure measured during the experiment [8]. The dashed lines indicate the numerical results obtained for the three different grid sizes. The numerical predictions of the evolution of pressure were consistent with the experimental results, and the nonlinear double peaks were reproduced correctly for all grid sizes through the CFD analyses. In addition, the grid size did

not significantly affect the numerical prediction. Therefore, this study used a coarse grid size of 0.01 m to limit the computation time.

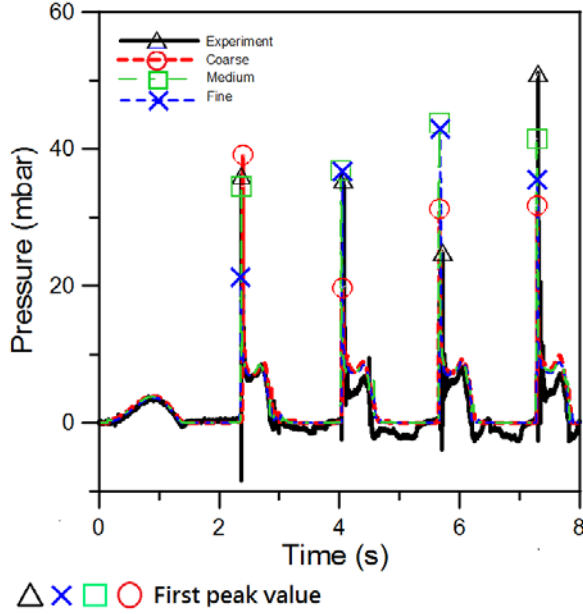


Figure 7. MESH SIZE VERIFICATION.

2.3 Rules sloshing load assessment

According to the rules [7], Eqs. (6) and (7) can compute the sloshing pressure over transverse bulkheads ($p_{bhd-lng}$) for longitudinal liquid motion and over longitudinal bulkheads (p_{bhd-t}) for transverse liquid motion, respectively.

$$p_{bhd-lng} = \rho g_0 l_s k_f \left[0.4 - \left(0.39 - \frac{1.7l_s}{L} \right) \frac{L}{350} \right] \quad (6)$$

$$p_{bhd-t} = 7 \rho g_0 k_f \left[\frac{b_s}{B} - 0.3 \right] GM^{0.75} \quad (7)$$

where g_0 is the standard acceleration of gravity (9.81 m/s^2), GM is the maximum metacentric height including correction for free surface effect, l_s is the effective sloshing length, b_s is the effective sloshing breadth, L is the ship length, B is the ship breadth and ρ is the density of liquid.

Equation (8) can compute the parameter k_f that corresponds to the amplitude of the sloshing pressure as a function of the filling ratio.

$$k_f = 1 - 2 \left(0.7 - \frac{h}{H} \right)^2 \quad (8)$$

where h is the filling height, and H is the tank height.

In Eq. (8), the maximum peak pressure is met for a filling ratio of 70%. The IACS [9] reported that the maximum sloshing pressure was reached at a filling ratio between 70% and 80%.

3. SIMULATION RESULTS

3.1 CFD settings

In Section 2.2, a time step of 0.001 s was found satisfactory for evaluating the sloshing pressure accurately; in addition, the accuracy of the numerical prediction was preserved for a coarse grid size of 0.01 m which corresponds to 50 elements through the depth of the small-scale model tank. According to this mesh size strategy, the cargo oil tanks considered were all meshed with a grid size that corresponds to 50 elements through the depth of the tank..

The rules [7] provide load formulations corresponding to sloshing in partially filled tanks containing seawater. Therefore, this study performed the CFD analyses by considering a liquid density and viscosity of 1.025 t/m^3 and $8.881 \times 10^{-4} \text{ Pa}\cdot\text{s}$, respectively.

Finally, this study conducted CFD analyses to evaluate the transverse and longitudinal sloshing loads in three cargo oil tanks selected from a handy-size oil tanker and VLCC. Four tank filling conditions, $h/H = \{30\%, 50\%, 70\%, \text{ and } 90\%\}$, were examined. These processes were conducted to study the considerations and technical background of the parameters defined in the formula. The results were compared with the rules loads to discuss the safety of rules and the basis of defined parameters.

3.2 Transverse sloshing in a handy size oil tanker COT

Table 1 lists the principal dimensions of the ship and the cargo oil tank located amidships.

Table 1. PRINCIPAL DIMENSIONS.

Ship dimensions	
Length between perpendiculars (L_{BP})	174 m
Breadth (B)	32.2 m
Depth (D)	17.3 m
Draft (T)	11 m
Cargo oil tank dimensions	
Tank length (L_T)	21.6 m
Tank breadth (B_T)	14.1 m
Tank height (H_T)	15.85 m

Figure 8 shows the geometry of the tank. Originally, the centerline and transverse bulkheads were composed of corrugated plates; however, this study adopted a simplified modeling approach assuming flat tank boundaries. The tank model was established as described in Section 3.1 and the model comprised 413509 cells with a grid size of 0.3 m. Eight sensors were also defined on the tank boundary corresponding to the inner hull at the tank mid-length. These sensors were installed to record the evolution associated with the transverse sloshing pressure.

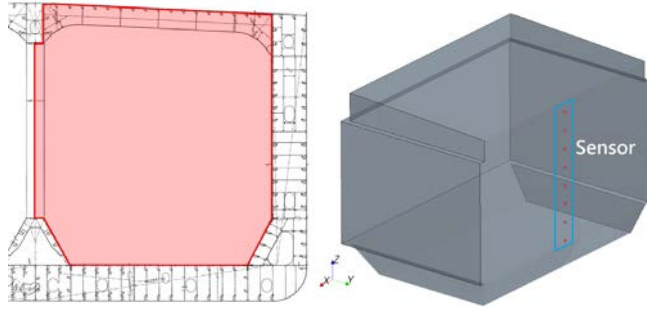


Figure 8. GEOMETRY OF THE CARGO OIL TANK LOCATED AMIDSHIP IN THE HANDY SIZE OIL TANKER.

The CFD sloshing simulations were then performed by imposing a periodic roll motion according to Eq. (5). To maximize the sloshing phenomenon, the frequency of the roll motion (ω) was set to correspond to the predicted fluid in the tank natural frequency (ω_r) that can be assessed based on the linear theory, as proposed by Faltinsen et al [10], using Eq. (9).

$$\omega_r = \sqrt{g \frac{\pi}{B_T} \tanh\left(\frac{\pi}{B_T} h\right)} \quad (9)$$

where B_T is the tank breadth, g is the acceleration of gravity (9.81 m/s^2), and h is the filling height.

This study subsequently defined the amplitude of the roll motion (θ_0) according to the CSR-H Rules by using Eq. (10), which can predict the maximum roll angle in the lifetime. Based on the rules, the predicted maximum roll angle obtained using Eq. (10) corresponded to a probability level of 10^{-8} , whereas the rules for sloshing loads were given for a probability level of 10^{-4} . Also, this study assumed that the long-term ship motion response corresponded to a two-parameter Weibull distribution with the shape parameter $k = 1$. Therefore, the amplitude of the roll motion (θ_0) was thus approximated to half the value provided by Eq. (10).

$$\theta_0 = \frac{9000 [1.25 - 0.025 T_\theta] f_p f_{BK}}{(B + 75)\pi} \quad (10)$$

$$T_\theta = \frac{2.3\pi k_r}{\sqrt{gGM}} \quad (11)$$

where T_θ is the roll period, f_p is the coefficient of strength assessment ($f_p = 1.0$ for extreme strength condition), f_{BK} is the coefficient of bilge keel ($f_{BK} = 1.0$ for ships with bilge keel), and k_r is the roll radius of gyration.

Table 2 lists the predicted fluid in tank natural frequency of transverse sloshing for the four filling cases examined and roll amplitude. The center of rotation was taken at the center of gravity of the ship as defined by the rules ship motions.

Table 2 ROLL MOTION PARAMETERS.

Filling ratio	Frequency (rad/s)	Amplitude (rad)
30%	1.312	0.214
50%	1.437	
70%	1.468	
90%	1.504	

Figure 9 shows the overturning wave free surface contour under each filling condition, indicating that the grid size is adequate for accurately reproducing the complex nonlinear behavior of the liquid during sloshing.

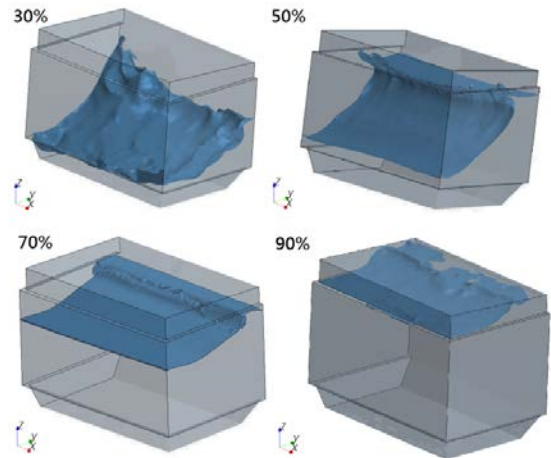


Figure 9 OVERTURNING WAVE FREE SURFACE CONTOUR FOR EACH FILLING LEVEL OF THE TANK.

This study assumed that the rules of sloshing pressure correspond to the peak value of the sloshing event. Therefore, the sloshing pressure was averaged over the peak values of six consecutive stable sloshing cycles among all cycles that were recorded during the simulation. Table 3 shows the predictions of the sloshing pressure obtained through CFD under all filling conditions. The maximum pressure over all sensors is marked in bold and the corresponding values of the rules are listed in the final row of the table for comparison. In addition, some sensors were constantly immersed during the simulation and thus did not record the sloshing pressure; these sensors instead recorded the quasistatic inertia load of the liquid. In Table 3, the cases for which the static pressure was subtracted from the total pressure to consider only the dynamic load component are marked with (*). Under each filling condition, the numerical prediction of the maximum sloshing pressure was close to the values of the rules which revealed that numerical results may be reasonable by these CFD settings. In addition, the maximum sloshing pressure was obtained under the 70% filling condition, which was consistent with the formulation of the rules (Section 2.3, Eq. (7)).

Table 3 MAXIMUM TRANSVERSE SLOSHING PRESSURE (kN/m²) RECORDED BY EACH SENSOR.

Sensor height Z (m)	Filling conditions			
	30%	50%	70%	90%
P2= 0.2 H	27.32	19.88 ^(*)	25.94 ^(*)	24.60 ^(*)
P3= 0.3 H	27.54	20.31	26.67 ^(*)	24.63 ^(*)
P4= 0.4 H	17.50	23.73	27.29 ^(*)	25.55 ^(*)
P5= 0.5 H	7.20	26.76	27.52	26.68 ^(*)
P6= 0.6 H	0	14.20	29.75	26.91 ^(*)
P7= 0.7 H	0	4.70	32.11	27.04 ^(*)
P8= 0.8 H	0	0	17.80	27.87
P9= 0.9 H	0	0	1.60	28.90
Rules sloshing pressure (p_{bhd-t} , see Eq. (6))	29.77	40.28	43.78	35.56
CFD/Rules	92.5%	65.7%	73.3%	81.3%

^(*) Quasistatic inertia load of the liquid

3.3 Transverse sloshing in a VLCC COT

Table 4 lists the principal dimensions of the ship and considered cargo oil tank located amidships.

Table 4 PRINCIPAL DIMENSIONS.

Ship dimensions	
Length between perpendiculars (L_{BP})	316 m
Breadth (B)	60 m
Depth (D)	29.7 m
Draft (T)	19.2 m
Cargo oil tank dimensions	
Tank length (L_T)	50.4 m
Tank breadth (B_T)	23.8 m
Tank height (H_T)	28.4 m

Figure 10 illustrates the geometry of the rectangular tank comprising longitudinal stiffeners on the deck and a longitudinal bulkhead as well as transverse primary supporting members such as cross-ties and deck transverse. However, this study adopted a simplified modeling approach assuming flat tank boundaries. The tank model was set as described in Section 3.1 and comprised 1625109 cells with a grid size of 0.3 m. Nine sensors were also defined on the tank boundary corresponding to the longitudinal bulkhead at the tank mid-length; these sensors were used to record the evolution of the transverse sloshing pressure.

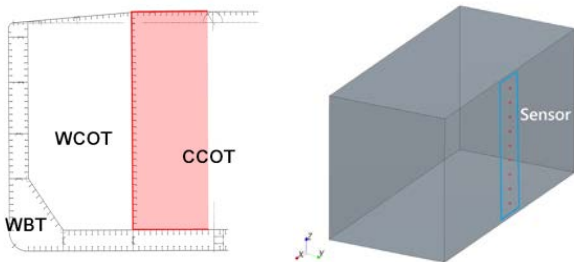


Figure 10. GEOMETRY OF THE CENTER CARGO OIL TANK LOCATED AMIDSHIP IN THE VLCC.

The process of determining the equation of roll motion of the simulation is presented in Section 3.2. Table 5 lists the predicted fluid in tank natural frequency of transverse sloshing for the four filling cases examined, and the roll amplitude. The center of rotation was taken at the center of gravity of the ship.

Table 5 ROLL MOTION PARAMETERS.

Filling ratio	Frequency (rad/s)	Amplitude (rad)
30%	1.023	0.148
50%	1.111	
70%	1.132	
90%	1.137	

Figure 11 shows, under each filling condition, the free surface contour of a traveling wave for 30% and 50% filling cases, an overturning wave for a 70% filling case, and a breaking wave over the tank top for a 90% filling case. As shown in this figure, the grid size is adequate for accurately reproducing the complex nonlinear behavior of the liquid during sloshing.

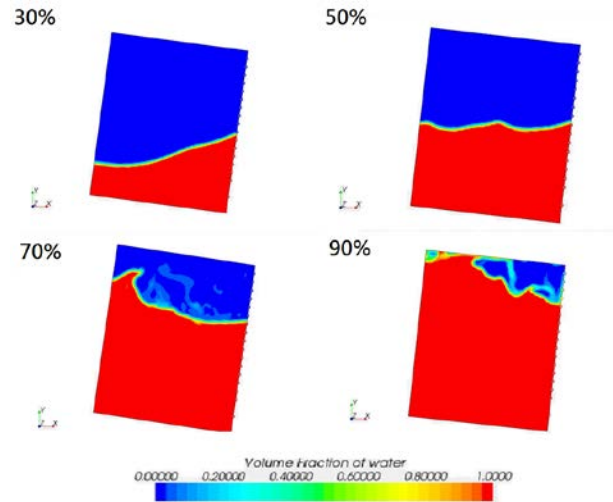


Figure 11 LIQUID FREE SURFACE CONTOUR FOR EACH FILLING LEVEL OF THE TANK.

Table 6 shows the predicted results of the sloshing pressure obtained by CFD under all filling conditions. The maximum pressure over all sensors is marked in bold and the corresponding pressure values of the rules are listed in the final row of the table for comparison. In addition, some sensors were constantly immersed during the simulation; thus these sensors did not record the sloshing pressure, and instead recorded the quasistatic inertia load of the liquid. In Table 6, the cases for which the static pressure was subtracted from the total pressure to consider only the dynamic load component are marked with (*). Under each filling condition, the numerical prediction of the maximum sloshing pressure was close to the values of the rules. In addition, the maximum sloshing pressure was obtained under the 70% filling condition, which was consistent with the

formulation of the rules (Section 2.3, Eq. (7)). As established by the rules [9], the sloshing pressure was higher near the free surface.

Table 6 MAXIMUM TRANSVERSE SLOSHING PRESSURE (kN/m²) RECORDED BY EACH SENSOR.

Sensor height Z (m)	Filling conditions			
	30%	50%	70%	90%
P1= 0.1 H	13.72 ^(*)	13.81 ^(*)	13.05 ^(*)	11.86 ^(*)
P2= 0.2 H	14.01 ^(*)	13.97 ^(*)	14.44 ^(*)	12.95 ^(*)
P3= 0.3 H	16.52	14.92 ^(*)	16.13 ^(*)	12.55 ^(*)
P4= 0.4 H	5.23	16.51 ^(*)	17.82 ^(*)	14.24 ^(*)
P5= 0.5 H	0	18.13	20.62 ^(*)	15.13 ^(*)
P6= 0.6 H	0	6.32	21.11	16.82 ^(*)
P7= 0.7 H	0	0	23.35	18.72 ^(*)
P8= 0.8 H	0	0	18.2	19.81
P9= 0.9 H	0	0	7.5	20.4
Rules sloshing pressure (p_{bhd-t} , see Eq. (6))	19.79	26.78	29.11	26.78
CFD/Rules	83.5%	67.7%	80.2%	76.2%

^(*) Quasistatic inertia load of the liquid

3.4 Longitudinal sloshing in a VLCC COT

The foremost center cargo oil tank No.1 was predicted to be subjected to the most severe longitudinal sloshing. Table 7 lists the principal dimensions of the considered cargo oil tank.

Table 7. PRINCIPAL DIMENSIONS.

Cargo oil tank dimensions	
Tank length (L_T)	50.4 m
Tank max breadth (B_T)	23.8 m
Tank height (H_T)	28.4 m

Figure 12 illustrates the geometry of the tank, which includes transverse primary support members such as cross ties and deck transverses. The tank model was created as described in Section 3.1 and comprised 2526015 cells with a grid size of 0.3 m. Nine sensors were also defined on the tank boundaries corresponding to the aft and fore transverse bulkhead at the centerline; these sensors were used to record the evolution of the longitudinal sloshing pressure.

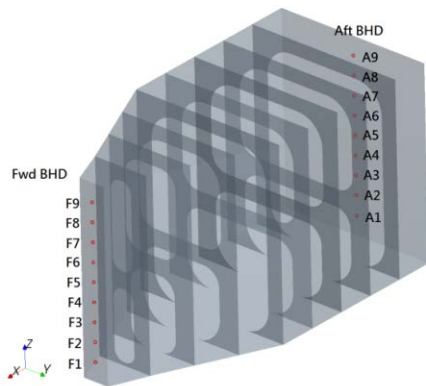


Figure 12. GEOMETRY OF THE CENTER CARGO OIL TANK IN THE FOREMOST PART OF THE VLCC

This study subsequently performed the CFD sloshing simulations by imposing a periodic pitch motion according to Eq. (12).

$$\varphi = \varphi_0 \sin \omega t \quad (12)$$

where φ is the angular position at time t , φ_0 is the maximum pitch angle corresponding to 0.054rad (i.e., approximately 3°) and ω is the pitch frequency.

To maximize the sloshing phenomenon, the frequency of the pitch motion (ω) was set to correspond to the predicted fluid in the tank natural frequency (ω_p) that can be assessed based on the linear theory, as proposed by Faltinsen et al [10], using Eq. (13).

$$\omega_p = \sqrt{g \frac{\pi}{L_T} \tanh\left(\frac{\pi}{L_T} h\right)} \quad (13)$$

where L_T is the tank length, g is the acceleration of gravity (9.81 m/s²), and h is the filling height.

This study then assessed the amplitude of the pitch motion (φ_0) according to the CSR-H by using Eq. (14), which can predict the maximum pitch angle in the lifetime. Based on the rules, the predicted maximum pitch angle obtained through Eq. (14) corresponded to a probability level of 10⁻⁸, whereas the rules for sloshing loads were given at a probability level of 10⁻⁴. Also, this study assumed that the long-term ship motion response corresponded to a two-parameter Weibull distribution with the shape parameter $k = 1$. Therefore, the amplitude of the pitch motion (φ_0) was approximated to half the value provided by Eq. (14).

$$\varphi_0 = 1350 f_p L^{-0.94} \left\{ 1.0 + \left(\frac{2.57}{\sqrt{gL}} \right)^{1.2} \right\} \quad (14)$$

$$T_\varphi = \sqrt{\frac{2\pi\lambda_\varphi}{g}} \quad (15)$$

$$\lambda_\varphi = 0.6(1 + f_T)L \quad (16)$$

where T_φ is the pitch period, f_p is the coefficient of strength assessment ($f_p = 1.0$ for extreme strength condition), and f_T is the ratio between draught at a loading condition and scantling draught which assuming $f_T = 1.0$.

Table 8 lists the predicted fluid in the tank natural frequency of longitudinal sloshing for the four filling cases examined, and the pitch amplitude. The center of rotation was taken at the center of gravity of the ship.

Table 8 PITCH MOTION PARAMETERS.

Filling ratio	Frequency (rad/s)	Amplitude (rad)
30%	0.545	
50%	0.658	0.054
70%	0.719	
90%	0.750	

Figure 13 shows the free surface contour of traveling waves for each filling case, indicating that the wave free surface contour was calm and therefore did not correspond to the sloshing. The predicted sloshing external motion for this tank configuration was likely inaccurate.

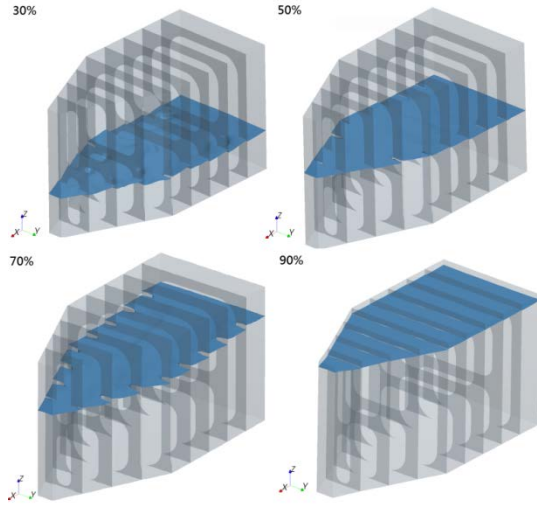


Figure 13 OVERTURNING WAVE FREE SURFACE CONTOUR FOR EACH FILLING LEVEL OF THE TANK.

Tables 9 and 10 show the predicted sloshing pressure obtained through CFD under all filling conditions. The maximum pressure over all sensors is marked in bold and the corresponding pressure values of the rules are listed in the final row of the table for comparison. In addition, some sensors were constantly immersed during the simulation; thus these sensors did not record the sloshing pressure, and they instead recorded the quasistatic inertia load of the liquid. In Table 9 and Table 10, the cases for which the static pressure was subtracted from the total pressure to consider only the dynamic load component are marked with (*). Both of the maximum value on the aft and forward bulkhead at filling condition 30% were slightly higher than those at 70% filling level. It is estimated that the cross-tie which may restrain free surface flow might had more significant effect on reducing sloshing loads at filling level 70% and 50%, and the value at 90% must be affected by the deck transverses (see fig13, case 90%) . For this case, the center of rotation was taken at the ship center of gravity and the transverse members generate discontinuities in the tank whereas Faltinsen formulation was established for a center of rotation taken in the middle of a tank considered with smooth

boundaries. This can explain the large deviation between rules and CFD predictions. For each filling condition, the numerical prediction of the maximum sloshing pressure was significantly lower than the values of the rules. However, Jeon et al [3] conducted a similar comparative study and concluded that the longitudinal sloshing pressure was overestimated in the CSR [7].

Table 9 MAXIMUM LONGITUDINAL SLOSHING PRESSURE (kN/m²) RECORDED BY EACH SENSOR ON THE AFT BULKHEAD.

Sensor height Z (m)	Filling conditions			
	30%	50%	70%	90%
A1= 0.1 H	11.29 ^(*)	7.18 ^(*)	17.27 ^(*)	12.27 ^(*)
A2= 0.2 H	19.00 ^(*)	7.79 ^(*)	17.98 ^(*)	12.97 ^(*)
A3= 0.3 H	25.30	8.39 ^(*)	18.28 ^(*)	13.37 ^(*)
A4= 0.4 H	9.30	9.80 ^(*)	20.89 ^(*)	13.98 ^(*)
A5= 0.5 H	0	10.45	21.19 ^(*)	14.18 ^(*)
A6= 0.6 H	0	4.20	22.20 ^(*)	14.99 ^(*)
A7= 0.7 H	0	0	24.20	15.29 ^(*)
A8= 0.8 H	0	0	5.80	15.70 ^(*)
A9= 0.9 H	0	0	0	16.20
Rules sloshing pressure (p_{bhd-l} , see Eq. (7))	54.15	60.28	70.98	68.13
CFD/Rules	46.7%	17.3%	34.1%	23.8%

^(*) Quasistatic inertia load of the liquid

Table 10 MAXIMUM LONGITUDINAL SLOSHING PRESSURE (kN/m²) RECORDED BY EACH SENSOR ON THE FORE BULKHEAD.

Sensor height Z (m)	Filling conditions			
	30%	50%	70%	90%
F1= 0.1 H	27.87 ^(*)	15.74 ^(*)	33.80 ^(*)	14.47 ^(*)
F2= 0.2 H	37.48 ^(*)	19.40 ^(*)	34.17 ^(*)	15.04 ^(*)
F3= 0.3 H	43.90	20.47 ^(*)	36.44 ^(*)	16.60 ^(*)
F4= 0.4 H	18.20	21.83 ^(*)	37.40 ^(*)	17.47 ^(*)
F5= 0.5 H	0	25.60	38.87 ^(*)	18.94 ^(*)
F6= 0.6 H	0	8.60	39.73 ^(*)	20.20 ^(*)
F7= 0.7 H	0	0	42.21	21.37 ^(*)
F8= 0.8 H	0	0	11.40	22.73 ^(*)
F9= 0.9 H	0	0	0	24.30
Rules sloshing pressure (p_{bhd-l} , see Eq. (7))	54.15	60.28	70.98	68.13
CFD/Rules	81.1%	42.5%	59.5%	35.7%

^(*) Quasistatic inertia load of the liquid

4. STRUCTURAL RESPONSE ASSESSMENT

This study investigated the structural response of stiffened panels subjected to sloshing. This study specifically considered three stiffened panels derived from each of the three previously examined tanks (Sections 3.2 to 3.4) at the 70% filling level. The stiffened panels were selected in way of the free surface of the liquid at which the sloshing pressure was the highest.

The stiffened panels FE model extent was set between the transverse web frames and horizontal girders, and the boundary

nodes were clamped to reproduce the effect of primary support members. Figures 14 to 16 illustrate the coupled CFD models and FE models of the stiffened panels No.1, No.2 and No.3 respectively.

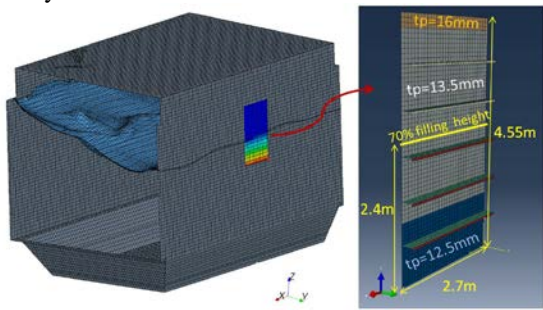


Figure 14 FLUID STRUCTURE INTERACTION MODEL OF THE STIFFENED PANEL LOCATED AMIDSHIPS IN A HANDY SIZE OIL TANKER SUBJECTED TO TRANSVERSE SLOSHING.

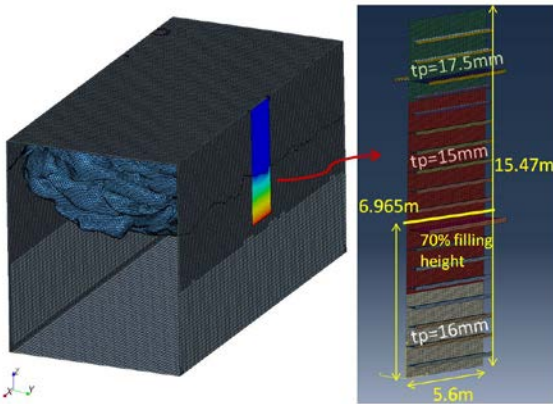


Figure 15 FLUID STRUCTURE INTERACTION MODEL OF THE STIFFENED PANEL LOCATED AMIDSHIPS IN A VLCC SUBJECTED TO TRANSVERSE SLOSHING.

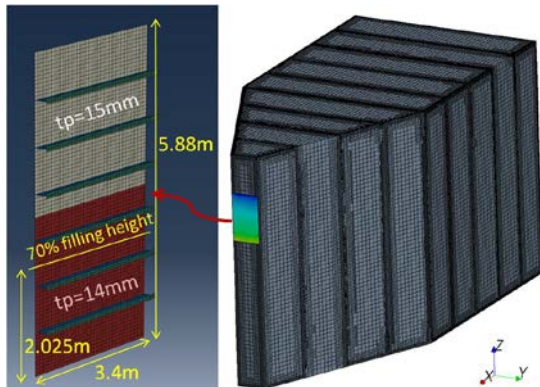


Figure 16 FLUID STRUCTURE INTERACTION MODEL OF THE STIFFENED PANEL LOCATED AMIDSHIPS IN A VLCC SUBJECTED TO LONGITUDINAL SLOSHING.

The structural response was examined through FSI analyses performed using ABAQUS and STARCCM+. Specifically, this study used the one-direction FSI method that

enabled directly transferring the hydrodynamic pressure obtained by CFD to the finite element model of the stiffened panel. The structural response during the sloshing event can thus be investigated by finite element analysis.

This study analyzed the structural response of the stiffened panels by using three loading approaches: dynamic sloshing pressure, static sloshing average pressure and static sloshing peak pressure. First, the FSI simulations were conducted over three cycles of dynamic sloshing pressures obtained by CFD analysis. The dynamic structural response was subsequently computed by carrying out implicit analysis. The static structural response to the peak pressure and the average pressure were also evaluated.

The left charts on Figures 17 to 19 show the dynamic sloshing pressures at 70% of the tank height for the three stiffened panels examined, the upper line corresponds to the peak pressure, whereas the lower line corresponds to the average pressure. The right charts on Figures 17 to 19 illustrate the corresponding dynamic structural response expressed in terms of lateral deflection; the upper line represents the static structural response to the average peak pressure corresponding to the quasistatic response to the sloshing pressure, whereas the lower line represents the static structure response to the average pressure corresponding to the impulsive response to the sloshing pressure.

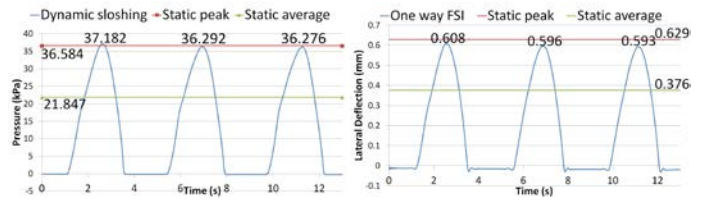


Figure 17 SLOSHING PRESSURE(LEFT) AND RESPONSE(RIGHT) OF STIFFENED PANEL1.

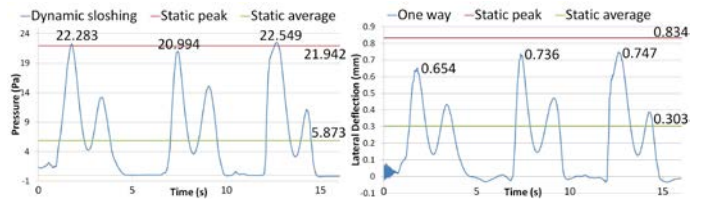


Figure 18 SLOSHING PRESSURE(LEFT) AND RESPONSE(RIGHT) OF STIFFENED PANEL2.

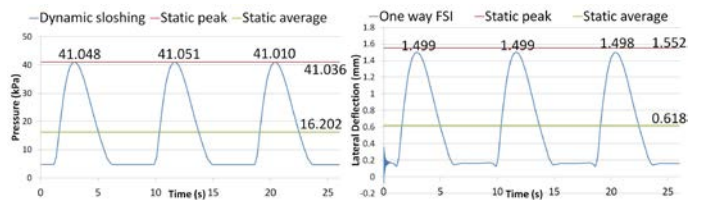


Figure 19 SLOSHING PRESSURE(LEFT) AND RESPONSE(RIGHT) OF STIFFENED PANEL3.

As shown in these figures, for all the examined stiffened panels, the dynamic response was slightly lower than the quasistatic response (upper line). Therefore, the dynamic response to the sloshing pressure can be considered quasistatic with some impulsive effect. The rules [7] quasistatic approach of the structural response to sloshing loads was thus reasonable.

NORSOK [11] categorizes the structural response according to the ratio of impact duration (t) to structural natural period (T):

- Quasi static domain: $3 \leq t/T$
- Dynamic or impact domain: $0.3 \leq t/T < 3$
- Impulsive domain : $t/T < 0.3$

The current study thus performed modal analysis for the three stiffened panels examined. Furthermore, the plates located at 70% of the tanks height were isolated by considering simply supported conditions at the edges where stand the stiffeners, and clamped conditions at both ends. The modal analysis of the plates enabled evaluating the natural period of the structure where the sloshing pressure was the largest (i.e. $z=70\%H_T$). Table 11 shows the results in terms of natural period, indicating that according to NORSOK criterion, the structural response of every stiffened panel is confirmed to be quasistatic.

Table 11. NATURAL PERIODS OF STIFFENED PANELS PANEL AND SLOSHING LOADS.

	SP-1	SP-2	SP-3
Sloshing Loads (t)	2.55s	3.41 s	5.13 s
Stiffened Panel (T)	0.016 s	0.054 s	0.019 s
t/T	159	63	270
Plate (T)	0.017 s	0.018 s	0.017 s
t/T	150	189	302

5. CONCLUSION

This study investigated the transverse sloshing in a cargo oil tank located amidships of a handysize oil tanker and VLCC, as well as the longitudinal sloshing in the foremost cargo oil tank of a VLCC. Furthermore, CFD analyses were performed to evaluate the sloshing pressure on the tank boundaries. The computation model was calibrated through a small-scale experiment. This study obtained the following findings:

1. For all investigated cases, the maximum sloshing load was obtained at the free surface under a 70% filling condition, as expressed in the formulation of the rules.
2. The predicted transverse sloshing pressure for the four filling levels were consistent with the values of the rules.

3. The longitudinal sloshing pressure predictions were significantly lower than the values of the rules. The formulation of tank natural frequency sloshing may not be applicable for tanks with large geometrical discontinuities such as those generated by transverse members. In addition, the surge and heave excitations were not considered although for this case they may have a significant effect on the prediction. The CFD settings should thus be further investigated for the longitudinal sloshing. However, other researchers have concluded on the conservativeness of the rules for this case.

The structural response to sloshing load was examined through a fluid structure analysis by combining CFD analysis and FEA. The analysis results indicated that the structural response was quasistatic with some impulsive effects, which validated the assumption in the rules of a quasistatic structural response to sloshing loads.

REFERENCES

- [1] Sames, P.C., Marcouly, D., and Schellin, T.E., 2002. "Sloshing in Rectangular and Cylindrical Tanks". *Journal of Ship Research*, Vol.46, No.3, pp.186-200.
- [2] Moirod, N., Baudin, E., Gazzola, T., Diebold, L., 2010. "Experimental and Numerical Investigations of the Global Forces Exerted by Fluid Motions on LNGC Prismatic tanks Boundaries". 20th ISOPE, China.
- [3] Jeon, S.S., Jung, J.H., Song, M.J., Ryu, M.C., Kim, Y.S., and Kim, S.E., 2012. "Comparative Study on the Effect of the Cross Tie on Sloshing Loads of a VLCC". 22nd ISOPE, Greece.
- [4] Fossa, M., Rizzo, C.M., Tani, G., and Viviani, M., 2012. "Simulations of a Sloshing Experiment by FEM CFD and FEM FSI Approaches". 22nd ISOPE, Greece.
- [5] Ganuga, R.S., Viswanathan, H., Sonar, S., and Awasthi, A., 2014. "Fluid-Structure Interaction Modelling of Internal Structures in a Sloshing Tank Subjected to Resonance". *International Journal of Fluid Mechanics Research*, Vol.41, No.2, pp. 145-168.
- [6] Pozarlik, A.K., Kok, J.B.W., 2007. "Numerical Investigation of One- and Two-way Fluid-Structure Interaction in Combustion Systems". International Conference on Computational Methods for Coupled Problems in Science and Engineering (COUPLED PROBLEMS 2007), Spain.
- [7] IACS, 2014. *Harmonized Common Structural Rules for Bulk Carriers and Oil Tankers*. IACS, London.
- [8] Souto-Iglesias, A., Botia-Vera, E., 2010. "SPHERIC benchmark test case-Wave impact problem". internal report, SPH European Research Interest Community, Spain.
- [9] IACS, 2012. *Technical Background Rule References for Harmonised CSR*. IACS, 1st November, London.
- [10] Faltinsen, O.M., Timokha, A.N., 2009. *Sloshing*, 1st ed., Cambridge University Press.
- [11] NORSOK, 2004. *N-004 Design of Steel Structure*. NORSOK